Environmental Science & Technology

Article

pubs.acs.org/est

Inland Sea Spray Aerosol Transport and Incomplete Chloride Depletion: Varying Degrees of Reactive Processing Observed during SOAS

Amy L. Bondy,[†] Bingbing Wang,[‡,¶] Alexander Laskin,[‡] Rebecca L. Craig,[†] Manelisi V. Nhliziyo,[§] Steven B. Bertman,[∥] Kerri A. Pratt,[†] Paul B. Shepson,[⊥] and Andrew P. Ault*[,†,#]

[†]Department of Chemistry, University of Michigan, Ann Arbor, Michigan 48109, United States

[‡]Environmental Molecular Sciences Laboratory, Pacific Northwest National Laboratory, Richland, Washington 99354, United States

[§]Department of Chemistry, Tuskegee University, Tuskegee, Alabama 36088, United States

[∥]Department of Chemistry, Western Michigan University, Kalamazoo, Michigan 49008, United States

[⊥]Departments of Chemistry and Earth, Atmospheric, and Planetary Sciences, Purdue University, West Lafayette, Indiana 47907, United States

[#]Department of Environmental Health Sciences, University of Michigan, Ann Arbor, Michigan 48109, United States

Supporting Information

ABSTRACT: Multiphase reactions involving sea spray aerosol (SSA) impact trace gas budgets in coastal regions by acting as a reservoir for oxidized nitrogen and sulfur species, as well as being a source of halogen gases (HCl, $ClNO_2$, etc.). Whereas most studies of multiphase reactions on SSA have focused on marine environments, far less is known about SSA transported inland. Herein, single-particle measurements of SSA are reported at a site >320 km from the Gulf of Mexico, with transport times of 7−68 h. Samples were collected during the Southern Oxidant and Aerosol Study (SOAS) in June−July 2013 near Centreville, Alabama. SSA was observed in 93% of 42 time periods analyzed. During two marine air mass periods, SSA represented significant number fractions of particles in the accumulation (0.2−1.0 μm, 11%) and coarse (1.0−10.0 μm, 35%) modes. Chloride content of SSA particles ranged from full to partial depletion, with 24% of SSA particles containing chloride (mole fraction of Cl/Na ≥ 0.1, 90% chloride depletion). Both the frequent observation of SSA at an inland site and the range of chloride depletion observed suggest that SSA may represent an underappreciated inland sink for NO_x/SO_2 oxidation products and a source of halogen gases.

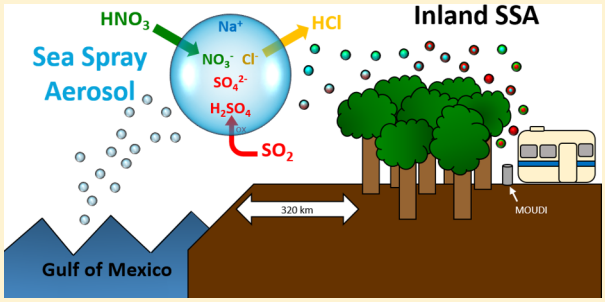

INTRODUCTION

Reactions of sea spray aerosol (SSA) with inorganic acids (HNO_3 and H_2SO_4) have long been observed in the polluted marine atmosphere and through controlled laboratory experiments.[1−26] Through multiphase reactions with key pollutants (NO_x and SO_2) and their oxidation products, SSA can impact nitrogen, sulfur, and oxidant budgets.[4,7,9,23,25,27,28] In addition to acting as a sink, particle-phase SSA reactions are also a source of halogen gases (HCl, Cl_2, $ClNO_2$, etc.).[13,26,29−33] A generalized acid reaction leading to the release of $HCl_{(g)}$ is shown in Reaction 1 where HA denotes atmospheric acids such as HNO_3, H_2SO_4, or CH_3SO_2OH.

$$HA_{(g,aq)} + NaCl_{(aq,s)} \rightarrow NaA_{(aq,s)} + HCl_{(g)} \quad (1)$$

Chloride displacement by liberation of $HCl_{(g)}$ in individual SSA has been observed from heterogeneous reactions of SSA with nitric acid.[2,13,30,32] This prominent SSA multiphase reaction has been widely studied and modeled.[2,13,17,19,21−23,30,34−38] Aged SSA may also contain sulfur species (in excess of seawater concentrations) due to reactions with H_2SO_4 or CH_3SO_2OH, formed from the oxidation of SO_2 or dimethyl sulfide (DMS), respectively.[3,19,39] Although not thermodynamically favored for bulk aqueous chemistry, SO_2 can be oxidized to H_2SO_4 in SSA because the oxidation of SO_2 occurs considerably faster than in pure water due to other oxidants (H_2O_2) or chloride ion catalysis.[15] More recently, laboratory and field studies have shown that NaCl can react with weak organic acids, such as malonic and citric acid, in addition to inorganic acids, releasing $HCl_{(g)}$.[40−42] Furthermore, SSA can undergo reactions with other reactive nitrogen gases such as N_2O_5 to form $NO_3^-{}_{(aq)}$ and $ClNO_{2(g)}$.[29,31,43−48] As SSA can react with a variety of species during transport, understanding the extent of processing by identifying the particle-phase reaction products formed when

Received: April 25, 2017
Revised: July 10, 2017
Accepted: July 21, 2017
Published: July 21, 2017

DOI: 10.1021/acs.est.7b02085
Environ. Sci. Technol. 2017, 51, 9533−9542

HCl is liberated is necessary for a thorough understanding of the multiphase chemistry experienced by SSA during transport to sites far from coastal environments.

Although SSA has been shown to act as an important sink for oxidized forms of NO_x and SO_2 in coastal regions, relatively few measurements have focused on SSA transported inland. Thus, the potential for inland SSA to have regional impacts after multiphase reactions, such as acting as a sink for HNO_3 and H_2SO_4 impacting nitrate deposition patterns,[49] is poorly understood.[50] To date, inland SSA has been detected with concentrations ranging from 1 to 20 $\mu g/m^3$ at locations 100 to >1000 km from their source in Israel,[51] Buenos Aires,[52] Ecuador,[53] Arkansas,[54] California,[41,55,56] Alaska,[57] Antarctica,[58,59] Spain,[60] Sweden,[61] and across the European continent[62] (Figure S1, Table S1). However, most sites are still somewhat close to the ocean (100−250 km) or in areas that are typically downwind of the ocean. Studies have relied primarily on bulk analysis methods, which use Cl^- or Na^+ concentrations, the ratio of Cl^-/Na^+, or the ratio of Cl^-/Mg^{2+} to identify SSA.[51−54,57−60,62] Whereas some studies detected only fresh SSA (since Cl^- was used as a marker),[51] aged SSA were detected in the majority of the studies using the Cl^-/Na^+ mass ratio which ranged from 0 to 1.8[52−54,57,58,60,61,63] (Cl^-/Na^+ = 1.81 in seawater).[64] Because $HCl_{(g)}$ can be released from SSA by the reactions discussed above, ratios involving Cl^- can lead to an underestimation of inland SSA concentrations.[23] Additionally, Na^+, Mg^{2+}, and Cl^- can also be present from other sources, such as mineral dust[65] and incineration,[66] further complicating the use of these ion ratios in bulk samples to accurately identify SSA.

Single-particle analysis overcomes challenges related to bulk average concentrations and ion ratios and allows for particle-by-particle comparison of SSA to seawater ion ratios, such as Na^+/Mg^{2+}.[1−3,11,39−41,67−73] By not using chloride to identify SSA, more detailed analysis of the extent of multiphase reactions that individual particles have undergone can be conducted. Scanning electron microscopy with energy dispersive X-ray spectroscopy (SEM-EDX) has been used extensively to identify fresh and aged SSA (SSA depleted in chloride), measure particle size and morphology, and analyze distributions of elements within individual particles.[1,3,37,40,41,71−78] SEM-EDX also has potential to provide a wealth of information regarding concentrations of SSA and the extent of aging at inland locations where few single-particle studies have been conducted.[41,55,56,79]

In this study, individual SSA particles were analyzed to determine the degree of aging as a function of particle size during the Southern Oxidant and Aerosol Study (SOAS) in 2013 near Centreville, Alabama. Computer-controlled SEM-EDX (CCSEM-EDX) was used to identify and analyze particles to determine elemental composition, size, and morphology. Computer-controlled Raman microspectroscopy (CC-Raman)[80] was used to identify secondary species (nitrate and sulfate) and trace organics. A previous SOAS publication investigated the impact of mineral dust aerosol on nitrate, but only briefly mentioned SSA influence.[79] Herein, two chemically distinct time periods with high SSA concentrations and different extents of aging were identified. Backward air mass trajectory analysis, in conjunction with weighted potential source contribution function analysis (WPSCF), and local meteorological data were used to investigate differences in atmospheric processing between these two SSA events. The presence of partially aged SSA transported inland may serve as sinks for HNO_3 and SO_2/H_2SO_4, as well as a source of oxidants in inland locations.

EXPERIMENTAL SECTION

Field Site Description and Sample Collection. Aerosol samples were collected as part of SOAS near Centreville, AL (32.9030 N, 87.2500 W, 242 m above mean sea level).[81] Centreville is located in a rural, forested region near Talladega National Forest approximately 320 km north of the Gulf of Mexico. Samples for single-particle analysis were collected between June 5 and July 11, 2013 near ground level (1 m) using a micro-orifice uniform deposit impactor (MOUDI, MSP Corp., model 110) sampling at 30 lpm with a PM_{10} cyclone (URG model 786). The 50% aerodynamic diameter size cut-points for the MOUDI sampling stages used in this analysis were 1.8, 1.0, 0.56, and 0.32 μm.[82] Particles were impacted onto 200-mesh carbon-type-B Formvar grids and quartz substrates (Ted Pella Inc.) for analysis with SEM-EDX and Raman spectroscopy, respectively. Samples were collected from 8:00−19:00 Central Standard Time (CST) and 20:00−7:00 CST, except during intensive periods when the schedule was 8:00−11:00, 12:00−15:00, 16:00−19:00, and 20:00−7:00 CST. Intensive time periods were scheduled based on predicted meteorological parameters and gas-phase concentrations.[83] After collection, all substrates were sealed and stored at −22 °C prior to analysis.

Computer-Controlled Scanning Electron Microscopy with Energy Dispersive X-ray Spectroscopy Analysis. Particles were analyzed using a FEI Quanta environmental SEM equipped with a field emission gun operating at 20 kV and a high-angle annular dark field (HAADF) detector.[72,84] The SEM was equipped with an EDX spectrometer (EDAX, Inc.). The CCSEM automated analysis captured single-particle physical parameters including projected area diameter and perimeter. EDX spectra from individual particles were analyzed to determine the relative abundance of 15 elements: C, N, O, Na, Mg, Al, Si, P, S, Cl, K, Ca, Ti, Fe, and Zn. For SOAS, a total of 34 266 particles were analyzed, including 4047 SSA particles. Single-particle data from the CCSEM-EDX analysis was examined in MATLAB R2013b (MathWorks, Inc.) using k-means clustering of individual particle EDX spectra following a previously described method.[85,86] Clusters were grouped by elemental composition into source-based classes, including SSA.[3,41,73] The particles identified as SSA in this study are unlikely to be influenced by other species such as dust, since the SSA particles were negligible in common soil elements, such as Si and Al. SSA data from two samples (July 4 20:00−July 5 7:00 and July 5 8:00−19:00) were excluded from analysis due to possible influence from fireworks.[87−89]

Computer-Controlled Raman Microspectroscopy. Raman microspectroscopy was performed using a Horiba LabRAM HR Evolution Raman spectrometer coupled with a confocal optical microscope (100× long working distance objective, Olympus). The instrument was equipped with a Nd:YAG laser source (50 mW, 532 nm), a charge-coupled device (CCD), and a 600 groove/mm diffraction grating (1.8 cm^{-1} spectral resolution). The instrument was calibrated daily using the Stokes Raman signal of pure Si at 521 cm^{-1}. The laser power was adjusted with a neutral density filter, and four accumulations (each with 15-s acquisition time) were used to collect spectra for the range of 500 to 4000 cm^{-1}. Approximately 200 particles (0.8−6.4 μm projected area diameter) from each SSA event (June 12, 2013 12:00−15:00 and July 4, 2013 8:00−19:00) were analyzed using CC-Raman to investigate secondary species, including nitrate, sulfate, and organics, using the method described by Craig et al.[80]

DOI: 10.1021/acs.est.7b02085
Environ. Sci. Technol. 2017, 51, 9533−9542

Hybrid Single-Particle Lagrangian Integrated Trajectory Model and Weighted Potential Source Contribution Function Analysis. The NOAA HYSPLIT model[90] was run at 100, 200, 500, 1000, and 3000 m (120 h backward) in conjunction with WPSCF receptor modeling[91] to examine the air mass histories of SSA during two SSA events: June 10−13, 2013 and July 3−8, 2013. Details about HYSPLIT and WPSCF analysis are provided in the Supporting Information.

RESULTS AND DISCUSSION

Individual SSA particles were identified during SOAS by the presence of sodium and magnesium in a ∼10:1 ratio (by atomic percent), which is equivalent to their molar ratio in seawater.[64] This fingerprint has been used to identify SSA in both laboratory and field studies using SEM-EDX, including both fresh and aged (depleted in chloride) SSA.[11,72,73,92] For EDX analysis it is typical to report atomic percentages of specific elements, which are equivalent to the mole percent of a specific element within the total particle. To facilitate comparison to bulk analyses, we report mole percentages and mole ratios in the analysis below. Details on identification of SSA through molar ratios are given in the Supporting Information and Table S2. Though primary biological and other organic particles have been observed to be emitted from marine environments,[70,93] due to their relatively smaller contributions and challenges differentiating these types of particles from organic or biological particles emitted from terrestrial sources at SOAS, only salt-containing SSA are discussed hereafter. Using CCSEM-EDX to identify SSA helps avoid misclassifying particles where Cl^- has been fully depleted via multiphase reactions. SSA particles identified during SOAS were classified into two categories: (1) partially aged (Cl/Na mole ratio ≥0.1) and (2) aged or fully processed (Cl/Na mole ratio <0.1). There is no "fresh" category of SSA, as no SSA particles were observed without some chloride depletion. Chloride enrichment factors, calculated by dividing the Cl^-/Na^+ mass ratio of the aerosol sample by the Cl^-/Na^+ ratio of seawater, are commonly used in ion chromatography to differentiate aged and fresh SSA.[94] However, the complete Cl loss in many particles made this approach impractical, and the simpler ratio of Cl/Na frequently used in EDX analysis,[41] is used herein. A molar threshold of 0.1 Cl/Na (1.16 in seawater) is used where particles with this ratio contain ≥10% of the chloride content (molar) of fresh SSA, and are therefore ≤90% depleted in chloride.

Within the fully aged category, particles were subclassified into sulfate-dominated (aged-sulfate, mole % S ≥ 1, mole % N < 1%) and mixed (aged-nitrate/sulfate, mole % S ≥ 1, mole % N ≥ 1). These thresholds were selected to minimize false positives due to background interferences. Figure 1 shows example images and EDX spectra of SSA particles from each of these three categories (partially aged, fully aged (aged-sulfate), and fully aged (aged-nitrate/sulfate)), with all three particles showing varying degrees of chloride depletion and the presence of nitrate and/or sulfate. For the elements Cl, N, and S associated with key anionic species (Cl^-, NO_3^-, SO_4^{2-}), in the representative particle from the partially aged class more Cl (9%) was present than N (2%) and S (2%) by mole %. In comparison, the two aged classes contain substantially less Cl, with the particle from the aged-sulfate class containing 0% Cl, 13% S, and 1% N, and the particle from the aged-nitrate/sulfate class containing 0% Cl, 3% S, and 2% N by mole %. Although EDX only measures elemental composition, whenever nitrogen and sulfur were present in the EDX spectra, elemental maps always showed collocation with oxygen,

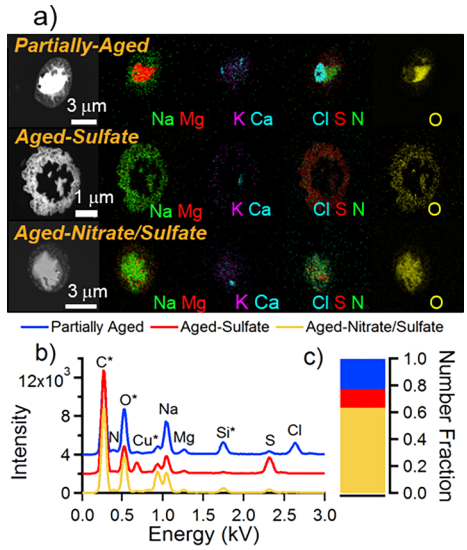

Figure 1. (a) SEM images and elemental maps of particles representing the three SSA classes observed during SOAS: partially aged, aged-sulfate, and aged-nitrate/sulfate, (b) corresponding EDX spectra, and (c) bar graph depicting the abundance of each SSA class by number fraction. Asterisk (*) indicates elements not quantitative due to interference from the substrate or detector. Standard error for the abundance of each class is below 0.01. A table with error values is located in SI Table S2.

suggesting that these elements were present in the form of nitrate and sulfate (Figure 1a). Raman microspectroscopy of particles from the same time period also showed frequent nitrate and sulfate vibrational modes, supporting this assignment (Figure S2). A future publication will focus on Raman mode analysis of particles from all sources at SOAS.

Elemental maps of particles representative of the three SSA classes in Figure 1a show the distribution of elements within each individual particle after impaction. In agreement with prior results,[1,95,96] the partially aged and aged SSA particles did not have elements homogeneously distributed spatially or a cubic efflorescence pattern typical of $NaCl_{(s)}$, suggesting the structures were not due to analysis under vacuum. Rather, spherical structures, some of which were core−shell, were observed. The distribution of elements with sodium, chloride (represented by Cl), and sulfate (represented by S) on the interior and magnesium and nitrate (represented by N) on the exterior is particularly apparent for the partially aged particle. In this particle, nitrate may have been enhanced at the surface, with chloride present within the core, due to reactions on an effloresced particle with a solid core. The enhancement of sodium rather than magnesium within the core suggests, unlike aged-nitrate/sulfate particles with the opposite cation organization, that the reaction was incomplete since cation rearrangement had not occurred.[1] Although three main classes of SSA were identified, a large variety of compositions and spatial distributions, even within a single particle category, were observed, necessitating an investigation of compositional variability.

The average EDX elemental percentages for all three types of SSA were observed to be depleted in chloride, although the extent of depletion varied, as shown in Figure 2. The partially aged class (24% of SSA by number) contained chloride in all the particles, with mole percentages of Cl ranging from 1 to 44%, with averages of 5% Cl, 2% S, and 5% N. Aged-sulfate particles (15% of SSA by number) were completely depleted in chloride

DOI: 10.1021/acs.est.7b02085
Environ. Sci. Technol. 2017, 51, 9533−9542

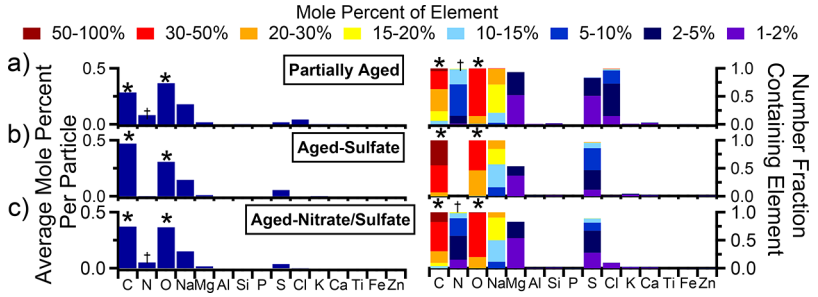

Figure 2. Average mole percent per particle and digital color histograms of three different particle classes of SSA: (a) partially aged, (b) aged-sulfate, and (c) aged-nitrate/sulfate. Average histograms are shown on the left as the elemental mole fraction across the elements analyzed by CCSEM-EDX. On the right, the digital color histogram heights represent the number fraction of particles containing a specific element, and the colors represent the mole percent of that element. Because analysis was conducted under vacuum, these mole percentages do not include moles of water. Asterisk (*) indicates elements (C, O) not quantitative due to interference from the substrate or detector, and (†) may have interfering signal from the carbon and oxygen EDX peaks.

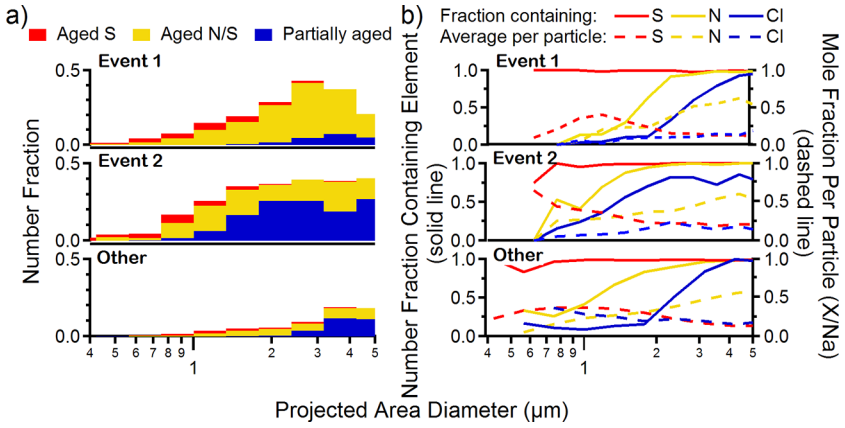

Figure 3. (a) Aged-sulfate, aged-nitrate/sulfate, and partially aged SSA depicted as a function of size during two SSA-rich periods: June 10−13 (Event 1), July 3−8 (Event 2), and throughout the rest of SOAS (other). During these two events, SSA is present at both submicron and supermicron sizes. (b) Size-resolved SSA composition indicates the number fraction of SSA containing Cl, N, and/or S. The solid line corresponds to the number fraction containing the element, while the dashed line corresponds to the mole fraction per particle relative to sodium.

and did not contain nitrate, but contained up to 15% S with an average of 6% S (mole %). Aged-nitrate/sulfate particles, which accounted for the majority (61% by number) of SSA analyzed, had minimal chloride (Cl/Na mole fraction <0.1) with nitrate and sulfate present in all particles (up to 15% N and S with an average of 5% N and 4% S by mole %). Less than 1% by number of SSA particles contained more than 10% Cl (with fresh SSA particles containing 49% Cl by mole percentage), indicating a substantial degree of processing during transport from the Gulf of Mexico.

During SOAS two events (Event 1: June 10−13 and Event 2: July 3−8) were identified that had high number percentages of SSA in the accumulation and coarse modes (11% and 35%, respectively), compared to the 6% median number percentage of SSA for all of the SOAS samples analyzed (Figure S3). During these events SSA are a substantial fraction of total $PM_{2.5}$ mass. The highly aged character from Figure 2 is supported by the mean pH of 0.9 ± 0.6 reported for $PM_{2.5}$ at the site.[97,98] When compared to the pH range of 7.0 to 9.0 which is typical for freshly emitted SSA,[26] HCl volatilization is predicted under these highly acidic conditions at Centreville,[26] though limited methods for direct pH determination are available.[99,100] To compare SSA aging during these events, the number fraction of SSA in each particle class was analyzed as a function of projected area diameter (Figure 3a). For comparison, the composition of SSA during the rest of the campaign, which accounted for approximately 20% of SSA by number, is also shown. For all SSA detected during SOAS, size plays an important role in chemical composition: sulfate-containing particles were present from 0.5 to 5 μm (stats were poor <0.5 μm), particles containing nitrate were mostly >1 μm, and partially aged particles containing chloride were generally >2 μm. Figure 3b shows the number fraction of particles containing any Cl, N, or S (mole percent >1%) in the particle. These data further support that within partially aged and aged SSA categories sulfate is concentrated in submicron particles, while chloride and nitrate are primarily in the supermicron size range. In addition to quantifying the number fraction of particles that contain nitrate, sulfate, and chloride, the average mole percent relative to sodium of each element was analyzed to determine their per particle concentrations as a function of size. Figure 3b shows that for all SSA, the number fraction of particles containing Cl increased with diameter with similar mole fractions of Cl (~0.2) within the largest particles analyzed. On the other hand, the mole fractions of N and S in SSA are inversely related. Whereas submicron particles are very S-rich, as diameter increases, the mole fraction of S within particles decreases and the mole fraction of N increases.

The size dependence of nitrate and sulfate within SSA particles provides insight into the mechanism for the uptake of HNO_3 and SO_2. In general, the accumulation of sulfate in SSA by reaction with SO_2 is diffusion limited. Therefore, it occurs most readily in

DOI: 10.1021/acs.est.7b02085
Environ. Sci. Technol. 2017, 51, 9533−9542

$PM_{2.5}$, particularly accumulation mode particles (diameters 0.1−1.0 μm).[35,36,63,101] Additionally, sulfate may accumulate in small particles because H_2SO_4, formed from the aqueous-phase or gas-phase oxidation of SO_2 in deliquesced particles and droplets, dissociates instantly to HSO_4^-, H^+, and SO_4^{2-} and stays in the particle phase after uptake or formation, as opposed to the higher vapor pressure HNO_3.[102] Over time, the accumulation of sulfate will acidify the particles, and more HNO_3 volatilization will lead to a "distillation effect" where more sulfate accumulates within the smaller particles and any pre-existing nitrate is displaced. Thus, NO_3^- will be present primarily in supermicron SSA,[23,35,36] preferentially particles ~1 μm since the net uptake for nitric acid onto NaCl is highest for micron-sized particles with large surface areas.[37] However, the reaction may not go to completion for large SSA since the uptake of HNO_3 is diffusion-limited above 1 μm,[37] leading to partially aged SSA particles. In short, the irreversible uptake of SO_2 on SSA is kinetically limited while the uptake of HNO_3 is kinetically limited for large particles and thermodynamically controlled for small particles, resulting in sulfate accumulation in submicron particles, and nitrate accumulation in supermicron particles.

In addition to composition varying as a function of size, SSA composition was different for the two events. During Event 1 in June, aged-nitrate/sulfate SSA accounted for the majority of SSA particles by number, consistent with work by Allen et al.,[79] who showed coarse particle nitrate was high from June 9−13 during SOAS. In contrast, during Event 2 the partially aged SSA particles account for the majority of SSA by number. For particles >4 μm, chloride is present in ≥70% of particles during both events. However, during Event 1, only 6% of submicron SSA, by number, contain chloride, while 33% of submicron SSA contain chloride during Event 2, showing different extents of chloride depletion. This high fraction of particles that are not fully depleted in chloride may have important implications for the nitrogen budget, with partially aged SSA acting as an inland sink for NO_x oxidation products.

Ternary diagrams (Figure 4) show percentages of Cl, N, and S with respect to the sum of Cl + N + S in individual particles by mole percent, as in eqs 2−4 shown below.

$$\mathrm{Cl\%} = \frac{\mathrm{Cl}}{\mathrm{Cl} + \mathrm{N} + \mathrm{S}} \times 100\% \quad (2)$$

$$\mathrm{N\%} = \frac{\mathrm{N}}{\mathrm{Cl} + \mathrm{N} + \mathrm{S}} \times 100\% \quad (3)$$

$$\mathrm{S\%} = \frac{\mathrm{S}}{\mathrm{Cl} + \mathrm{N} + \mathrm{S}} \times 100\% \quad (4)$$

These plots highlight differences in aging processes between the SSA events. During Event 1 two populations are observed: (1) particles containing varying amounts of N and S with complete Cl depletion, and (2) particles containing varying amounts of N and Cl with minimal S. As also shown in Figure 3b, Cl is in the largest particles and the largest S enrichments are in the smallest particles, with lower relative mole fractions of S (1−2%) observed in particles >2.5 μm (although all particles 0.5−5 μm contained some amount of S). High relative percentages of N (≥60%) are found in all SSA ≥1 μm, suggesting particles were within a favorable size range for maximal uptake of HNO_3. In comparison, during Event 2, particles were smaller than the first event with average diameters <2.5 μm, and contained less N relative to S and Cl. To highlight the variation of N, the average relative percentages of N, S, and Cl were calculated for each

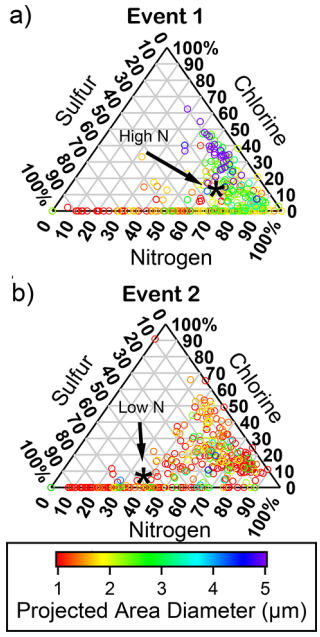

Figure 4. Ternary plots showing the relative percent of sulfate (S), chloride (Cl), and nitrate (N) in individual SSA particles collected from SOAS as a function of particle diameter for (a) Event 1 and (b) Event 2. Only every 5th (Event 1) or 3rd (Event 2) particle, respectively, is shown on the plots to better show trends. The asterisk (*) shows the average SSA composition during each event, with SSA from Event 1 containing substantially more nitrogen than SSA from Event 2.

event, represented by the asterisks in Figure 4. The average N% is much higher during Event 1 (65%) than during Event 2 (36%), indicating that SSA during this event were aged to a greater extent by HNO_3. Conversely, the average mole percentage of S increased (21% during Event 1 to 56% during Event 2), and Cl remained approximately constant (13% during Event 1, 8% during Event 2), even though the particles were much smaller during Event 2. The presence of chloride in a higher number fraction during Event 2, particularly in SSA <2.5 μm, may suggest an inhibition of multiphase reactions due to the particles not behaving as ideal aqueous droplets (e.g., effloresced particles or particles coated with organic material inhibiting uptake)[103] or transport at higher altitudes with lower HNO_3 and SO_2 concentrations.

To examine the air mass history during the two high-SSA events, HYSPLIT analysis with WPSCF was used. Shown in Figure 5, the SSA collected at rural, forested Centreville originated from the Gulf of Mexico and were transported inland. However, throughout these two SSA events, the particles arrived at Centreville via different transport routes, speeds, and altitudes. During Event 1, the air mass arrived from the southwest after passing over Louisiana and Mississippi; while during Event 2, the air mass approached Centreville directly from the south after traveling over Alabama and the Florida panhandle. Figure 5c shows example HYSPLIT backward air mass trajectories from Event 1, where the air mass spends ~24 h over land, while the backward air mass trajectories for Event 2 only spent ~10 h over land. The air masses from Event 1 traveled within the boundary layer over land, but due to differences in chemical composition from aerosol emitted from freshwater,[104,105] we are confident these particles are of marine origin and not from lakes or rivers the air mass passed over en route to Centreville. In contrast to Event 1, the air mass influencing Event 2 was primarily in the free

DOI: 10.1021/acs.est.7b02085
Environ. Sci. Technol. 2017, 51, 9533−9542

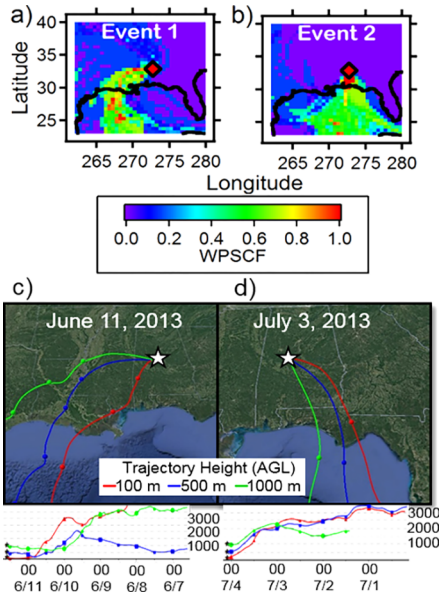

Figure 5. WPSCF trajectory analysis of SSA for (a) Event 1 and (b) Event 2 ending at Centreville, AL. WPSCF data are shown for SSA >6% (median % SSA during SOAS) by number according to CCSEM-EDX analysis and clustering. Example HYSPLIT 120-h backward air mass trajectories during Event 1 ending at Centreville on (c) June 11, 2013 at 8:00 and Event 2, (d) July 3, 2013 at 20:00. The red trajectory corresponds with trajectories ending at 100 m AGL, blue with 500 m AGL, and green with 1000 m AGL. *Circles on trajectory are spaced 12 h apart. Map data for c and d copyright Google, Image Landsat/ Copernicus; data from SIO, NOAA, U.S. Navy, NGA, GEBCO.

troposphere until the last few hours prior to arrival at Centreville. Although the transport time from the Gulf of Mexico was 2−3 times longer for the more aged SSA Event 1, exposure to different pollutant levels on the two trajectories, rather than diffusion-limited reactions over the transport time scale, likely led to the differences in SSA composition. To support this, the theoretical uptake of HNO_3 onto SSA completely aging particles was calculated to take ∼4 h (Table S3), which is much shorter than the transport times of particles during SOAS, particularly during Event 1. Meteorological data indicated that immediately preceding Event 2, Centreville experienced heavy rainfall[106,107] leading to a reduction of gaseous HNO_3,[79] while Event 1 SSA experienced no precipitation. Specifically, Event 2 gas-phase measurements of NO_y (0.51 ppb) and HNO_3 (0.03 ppb) were much lower compared to concentrations of NO_y (1.28 ppb) and HNO_3 (0.23 ppb) during Event 1 (Figure S4), which may be indicative of changes in regional NO_y and HNO_3 concentrations along the transport paths though values likely vary along the trajectory to the site. The high concentrations of HNO_3 and NO_y during Event 1 may account for the highly nitrate-aged SSA analyzed during that period, compared to the high concentrations of partially aged SSA detected during Event 2.

The importance of transport time for predicting whether chloride has been fully depleted from a particle is shown in Figure 6 by the average chloride depletion in SSA (mole %) as a function of air mass transport time from the Gulf (% Cl depletion calculations in Supporting Information). During Event 1, SSA experienced much longer transport times, with 30 h median transport times from the ocean based on backward air mass trajectories 500 m above ground level (Figure 5a). Air masses that were transported for 20−29 h contained slightly more chloride (98% Cl depleted, by mole %) compared to air masses

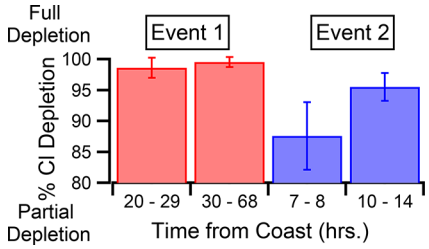

Figure 6. Average mole % of chloride depleted from SSA particles after transport from the ocean during Event 1 and Event 2. Five sampling times were averaged for each category during Event 1, and two and three sampling times were averaged for the Event 2 categories, respectively. Error bars represent one standard deviation from the mean. The time from the coast is calculated in hours using HYSPLIT.

that had transport times of 30−68 h (99% Cl depleted), although the difference is not statistically significant (Table S4), suggesting the reactions were not diffusion-limited on these time scales. By comparison, SSA during Event 2 had a median transport time of 10 h over land and contained substantially more chloride. Air masses with transport times of 7−8 h were on average 87% chloride depleted (mole %), which is statistically different at the 90% confidence interval from the 95% chloride depletion of SSA that traveled over land for more than 10 h. Thus, the combination of transport time and heavy precipitation leading to wet deposition of NO_y species likely caused differing chloride levels during the two SSA events.

To estimate the maximum contribution of SSA chloride depletion on the atmospheric oxidant budget, the mass of chlorine released during transport during Event 1 was calculated. First, the SSA mass concentration was calculated based on the Na^+ concentration (μmol/m^3) measured using a monitor for aerosols and gases (MARGA) at the Centreville site,[79] shown by CCSEM-EDX to be SSA. The seawater Cl^-/Na^+ ratio (1.81)[64] was applied to calculate the original Cl^- concentration, and an average of 98% (mole) chloride depletion, as determined by CCSEM-EDX (Figure 6), was applied to calculate moles of chlorine that partitioned to the gas phase during transport. During Event 1, when most chloride was depleted, a maximum of ∼620 ppt of HCl (17 μmol/m^3 Cl; from 15 μmol/m^3 of Na^+) is released into the atmosphere. Considering much lower concentrations of HCl (∼180 ppt during this same time period) were measured at the Centreville site,[79] most HCl (or Cl_2, $ClNO_2$) was likely released during transport from the ocean. These results indicate that under specific conditions, SSA may act as a source of Cl inland modifying the oxidant budget, and, if complete depletion does not occur during transport, SSA may exist as a source of HCl and a sink for oxidized NO_x species at inland locations.

Atmospheric Implications. SSA impact atmospheric chemistry and climate as they undergo multiphase reactions in the atmosphere, thereby acting as sinks for NO_x oxidation products and SO_2 as well as a source of gaseous halogen species (e.g., HCl and $ClNO_2$).[4−9,108] During the summer 2013 SOAS field campaign in Centreville, Alabama, SSA particles comprised up to 81% of supermicron (1−10 μm) and 48% of submicron (0.2−1.0 μm) particles, by number, during two multiday events. Because Centreville, AL is an inland site located approximately 320 km from the coast, most of the SSA was depleted in chloride and enriched in nitrate and sulfate due to transport and reactions with acidic species. Still, 24% of all SSA particles sampled, by number, contained detectable chloride (Cl/Na mole ratio ≥0.1),

DOI: 10.1021/acs.est.7b02085
Environ. Sci. Technol. 2017, 51, 9533−9542

suggesting that complete chloride depletion frequently did not occur. During Event 2, shorter transport times and subsidence from aloft during periods of low $HNO_{3(g)}$ led to particles where less than 90% of chloride had been depleted, although additional factors, such as the presence of an organic coating, could have impacted SSA reactivity during transport.

The findings suggest chloride-containing SSA existing at inland sites may have important implications for the nitrogen and oxidant budgets in the southeast U.S. or other inland sites, as these SSA will likely undergo further reactions during continued transport inland. Thus, SSA may act as an underappreciated inland sink for NO_x and SO_2 oxidation products, and source of reactive halogen-containing gases. Additionally, SSA could act as an inland cloud condensation nuclei source, indirectly impacting climate through cloud formation. The outcomes of this study provide insight regarding secondary chemistry involving aerosols in the southeast U.S. Additional studies at inland sites, particularly less-polluted ones, are needed to examine effects on oxidation products of NO_x, SO_2, and the oxidant budget from halogen production.

■ ASSOCIATED CONTENT

Supporting Information

The Supporting Information is available free of charge on the ACS Publications website at DOI: 10.1021/acs.est.7b02085.

Additional information on previous inland SSA studies, HYSPLIT and PSCF parameters, identification of SSA, CC-Raman analysis, selection of two SSA events, theoretical HNO_3 uptake calculation, HNO_3 and NO_y concentration plots, equation for chloride depletion, and Student *t* test equations and results (PDF)

■ AUTHOR INFORMATION

Corresponding Author

*Phone: 734-763-4212; e-mail: aulta@umich.edu; mail: 1415 Washington Heights, Ann Arbor, MI 48109.

ORCID

Alexander Laskin: 0000-0002-7836-8417

Kerri A. Pratt: 0000-0003-4707-2290

Andrew P. Ault: 0000-0002-7313-8559

Present Address

¶State Key Laboratory of Marine Environmental Science, College of Ocean and Earth Sciences, Xiamen University, Xiamen, China.

Notes

The authors declare no competing financial interest.

■ ACKNOWLEDGMENTS

We acknowledge EPA (R835409) for SOAS sampling funding. CCSEM was performed at the Environmental Molecular Sciences Laboratory (EMSL), a science user facility located at Pacific Northwest National Laboratory (PNNL), sponsored by the Office of Biological and Environmental Research. PNNL is operated for the U.S Department of Energy by Battelle Memorial Institute under contract DE-AC06-76RL0 1830. Travel funds to PNNL were provided by UM Rackham Graduate School and the UM Office of the Provost. We wish to thank the Southeastern Aerosol Research and Characterization (SEARCH) program for NO_y and HNO_3 measurements. Additionally, we thank Annmarie Carlton (Rutgers University, now UC-Irvine), Lindsay Yee (UC-Berkeley), Jason Surratt (UNC-Chapel Hill), and Allen Goldstein (UC-Berkeley) for organizing SOAS and the filter sampling effort, as well as Karsten Baumann and others for logistical assistance.

■ REFERENCES

(1) Ault, A. P.; Guasco, T. L.; Ryder, O. S.; Baltrusaitis, J.; Cuadra-Rodriguez, L. A.; Collins, D. B.; Ruppel, M. J.; Bertram, T. H.; Prather, K. A.; Grassian, V. H. Inside versus outside: ion redistribution in nitric acid reacted sea spray aerosol particles as determined by single particle analysis. *J. Am. Chem. Soc.* **2013**, *135* (39), 14528−14531.

(2) Gard, E. E.; Kleeman, M. J.; Gross, D. S.; Hughes, L. S.; Allen, J. O.; Morrical, B. D.; Fergenson, D. P.; Dienes, T.; Galli, M. E.; Johnson, R. J.; Cass, G. R.; Prather, K. A. Direct observation of heterogeneous chemistry in the atmosphere. *Science* **1998**, *279* (5354), 1184−1187.

(3) Hopkins, R. J.; Desyaterik, Y.; Tivanski, A. V.; Zaveri, R. A.; Berkowitz, C. M.; Tyliszczak, T.; Gilles, M. K.; Laskin, A. Chemical speciation of sulfur in marine cloud droplets and particles: analysis of individual particles from the marine boundary layer over the California current. *J. Geophys. Res.*. **2008**, *113*, (D4); DOI: 10.1029/2007JD008954.

(4) De Haan, D. O.; Brauers, T.; Oum, K.; Stutz, J.; Nordmeyer, T.; Finlayson-Pitts, B. J. Heterogeneous chemistry in the troposphere: experimental approaches and applications to the chemistry of sea salt particles. *Int. Rev. Phys. Chem.* **1999**, *18* (3), 343−385.

(5) Ravishankara, A. R.; Longfellow, C. A. Reactions on tropospheric condensed matter. *Phys. Chem. Chem. Phys.* **1999**, *1* (24), 5433−5441.

(6) Reid, J. P.; Sayer, R. M. Chemistry in the clouds: the role of aerosols in atmospheric chemistry. *Sci. Prog.* **2002**, *85* (3), 263.

(7) Rossi, M. J. Heterogeneous reactions on salts. *Chem. Rev.* **2003**, *103* (12), 4823−4882.

(8) Gibson, E. R.; Hudson, P. K.; Grassian, V. H. Physicochemical properties of nitrate aerosols: implications for the atmosphere. *J. Phys. Chem. A* **2006**, *110* (42), 11785−11799.

(9) Finlayson-Pitts, B. J. Reactions at surfaces in the atmosphere: integration of experiments and theory as necessary (but not necessarily sufficient) for predicting the physical chemistry of aerosols. *Phys. Chem. Chem. Phys.* **2009**, *11* (36), 7760−7779.

(10) Allen, H. C.; Laux, J. M.; Vogt, R.; Finlayson-Pitts, B. J.; Hemminger, J. C. Water-induced reorganization of ultrathin nitrate films on NaCl: Implications for the tropospheric chemistry of sea salt particles. *J. Phys. Chem.* **1996**, *100* (16), 6371−6375.

(11) Ault, A. P.; Guasco, T. L.; Baltrusaitis, J.; Ryder, O. S.; Trueblood, J. V.; Collins, D. B.; Ruppel, M. J.; Cuadra-Rodriguez, L. A.; Prather, K. A.; Grassian, V. H. Heterogeneous reactivity of nitric acid with nascent sea spray aerosol: large differences observed between and within individual particles. *J. Phys. Chem. Lett.* **2014**, *5* (15), 2493−2500.

(12) Duce, R. A. On source of gaseous chlorine in marine atmosphere. *J. Geophys. Res.* **1969**, *74* (18), 4597−4599.

(13) Robbins, R. C.; Cadle, R. D.; Eckhardt, D. L. The conversion of sodium chloride to hydrogen chloride in the atmosphere. *J. Meteorol.* **1959**, *16* (1), 53−56.

(14) Martens, C. S.; Wesolowski, J. J.; Harriss, R. C.; Kaifer, R. Chlorine loss from Puerto Rican and San Francisco Bay area marine aerosols. *J. Geophys. Res.* **1973**, *78* (36), 8778−8792.

(15) Clarke, A. G.; Radojevic, M. Oxidation rates of SO_2 in sea-water and sea-salt aerosols. *Atmos. Environ.* **1984**, *18* (12), 2761−2767.

(16) Okada, K.; Ishizaka, Y.; Masuzawa, T.; Isono, K. Chlorine deficiency in coastal aerosols. *J. Meteorol. Soc. Jpn.* **1978**, *56* (5), 501−507.

(17) Mamane, Y.; Gottlieb, J. Heterogeneous reaction of nitrogen oxides on sea salt and mineral particles—a single particle approach. *J. Aerosol Sci.* **1990**, *21*, S225−S228.

(18) Mamane, Y.; Mehler, M. On the nature of nitrate particles in a coastal urban area. *Atmos. Environ.* **1987**, *21* (9), 1989−1994.

(19) McInnes, L. M.; Covert, D. S.; Quinn, P. K.; Germani, M. S. Measurements of chloride depletion and sulfur enrichment in individual sea-salt particles collected from the remote marine boundary layer. *J. Geophys. Res.* **1994**, *99* (D4), 8257−8268.

DOI: 10.1021/acs.est.7b02085
Environ. Sci. Technol. 2017, 51, 9533−9542

(20) Sievering, H.; Boatman, J.; Galloway, J.; Keene, W.; Kim, Y.; Luria, M.; Ray, J. Heterogeneous sulfur conversion in sea-salt aerosol particles-the role of aerosoll water-content and size distribution. *Atmos. Environ., Part A* **1991**, *25* (8), 1479−1487.
(21) Cadle, R. D. Formation and chemical reactions of atmospheric particles. *J. Colloid Interface Sci.* **1972**, *39* (1), 25−31.
(22) ten Brink, H. M. Reactive uptake of HNO_3 and H_2SO_4 in sea-salt (NaCl) particles. *J. Aerosol Sci.* **1998**, *29* (1), 57−64.
(23) Pakkanen, T. A. Study of formation of coarse particle nitrate aerosol. *Atmos. Environ.* **1996**, *30* (14), 2475−2482.
(24) O'Dowd, C. D.; Smith, M. H.; Consterdine, I. E.; Lowe, J. A. Marine aerosol, sea-salt, and the marine sulphur cycle: a short review. *Atmos. Environ.* **1997**, *31* (1), 73−80.
(25) Ravishankara, A. R. Heterogeneous and multiphase chemistry in the troposphere. *Science* **1997**, *276* (5315), 1058−1065.
(26) Keene, W. C.; Pszenny, A. A. P.; Jacob, D. J.; Duce, R. A.; Galloway, J. N.; Schultz-Tokos, J. J.; Sievering, H.; Boatman, J. F. The geochemical cycling of reactive chlorine through the marine troposphere. *Global Biogeochem. Cycles* **1990**, *4* (4), 407−430.
(27) Schroeder, W. H.; Urone, P. Formation of nitrosyl chloride from salt particles in air. *Environ. Sci. Technol.* **1974**, *8* (8), 756−758.
(28) Pósfai, M.; Anderson, J. R.; Buseck, P. R.; Shattuck, T. W.; Tindale, N. W. Constituents of a remote pacific marine aerosol: a TEM study. *Atmos. Environ.* **1994**, *28* (10), 1747−1756.
(29) Finlayson-Pitts, B. J.; Ezell, M. J.; Pitts, J. N. Formation of chemically active chlorine compounds by reactions of atmospheric NaCl particles with gaseous N_2O_5 and $ClONO_2$. *Nature* **1989**, *337* (6204), 241−244.
(30) Eldering, A.; Solomon, P. A.; Salmon, L. G.; Fall, T.; Cass, G. R. Hydrochloric acid-a regional perspective on concentrations and formation in the atmosphere of southern California. *Atmos. Environ., Part A* **1991**, *25* (10), 2091−2102.
(31) Roberts, J. M.; Osthoff, H. D.; Brown, S. S.; Ravishankara, A. R. N_2O_5 oxidizes chloride to Cl_2 in acidic atmospheric aerosol. *Science* **2008**, *321* (5892), 1059−1059.
(32) Clegg, S. L.; Brimblecombe, P. Potential degassing of hydrogen chloride from acidified sodium chloride droplets. *Atmos. Environ.* **1985**, *19* (3), 465−470.
(33) Dasgupta, P. K.; Campbell, S. W.; Al-Horr, R. S.; Ullah, S. M. R.; Li, J.; Amalfitano, C.; Poor, N. D. Conversion of sea salt aerosol to $NaNO_3$ and the production of HCl: analysis of temporal behavior of aerosol chloride/nitrate and gaseous HCl/HNO_3 concentrations with AIM. *Atmos. Environ.* **2007**, *41* (20), 4242−4257.
(34) Roth, B.; Okada, K. On the modification of sea-salt particles in the coastal atmosphere. *Atmos. Environ.* **1998**, *32* (9), 1555−1569.
(35) Kerminen, V. M.; Teinila, K.; Hillamo, R.; Pakkanen, T. Substitution of chloride in sea-salt particles by inorganic and organic anions. *J. Aerosol Sci.* **1998**, *29* (8), 929−942.
(36) Zhuang, H.; Chan, C. K.; Fang, M.; Wexler, A. S. Formation of nitrate and non-sea-salt sulfate on coarse particles. *Atmos. Environ.* **1999**, *33* (26), 4223−4233.
(37) Liu, Y.; Cain, J. P.; Wang, H.; Laskin, A. Kinetic study of heterogeneous reaction of deliquesced NaCl particles with gaseous HNO_3 using particle-on-substrate stagnation flow reactor approach. *J. Phys. Chem. A* **2007**, *111* (40), 10026−10043.
(38) Saul, T. D.; Tolocka, M. P.; Johnston, M. V. Reactive uptake of nitric acid onto sodium chloride aerosols across a wide range of relative humidities. *J. Phys. Chem. A* **2006**, *110* (24), 7614−7620.
(39) Gaston, C. J.; Pratt, K. A.; Qin, X.; Prather, K. A. Real-time detection and mixing state of methanesulfonate in single particles at an inland urban location during a phytoplankton bloom. *Environ. Sci. Technol.* **2010**, *44* (5), 1566−1572.
(40) Ghorai, S.; Wang, B.; Tivanski, A.; Laskin, A. Hygroscopic properties of internally mixed particles composed of NaCl and water-soluble organic acids. *Environ. Sci. Technol.* **2014**, *48* (4), 2234−2241.
(41) Laskin, A.; Moffet, R. C.; Gilles, M. K.; Fast, J. D.; Zaveri, R. A.; Wang, B.; Nigge, P.; Shutthanandan, J. Tropospheric chemistry of internally mixed sea salt and organic particles: surprising reactivity of NaCl with weak organic acids. *J. Geophys. Res.: Atmos.* **2012**, *117*, No. D15302.
(42) Wang, B.; O'Brien, R. E.; Kelly, S. T.; Shilling, J. E.; Moffet, R. C.; Gilles, M. K.; Laskin, A. Reactivity of liquid and semisolid secondary organic carbon with chloride and nitrate in atmospheric aerosols. *J. Phys. Chem. A* **2015**, *119* (19), 4498−4508.
(43) Thornton, J. A.; Abbatt, J. P. D. N_2O_5 reaction on submicron sea salt aerosol: kinetics, products, and the effect of surface active organics. *J. Phys. Chem. A* **2005**, *109* (44), 10004−10012.
(44) Woods, E., III; Heylman, K. D.; Gibson, A. K.; Ashwell, A. P.; Rossi, S. R. Effects of NO_y aging on the dehydration dynamics of model sea spray aerosol. *J. Phys. Chem. A* **2013**, *117* (20), 4214−4222.
(45) Ryder, O. S.; Ault, A. P.; Cahill, J. F.; Guasco, T. L.; Riedel, T. P.; Cuadra-Rodriguez, L. A.; Gaston, C. J.; Fitzgerald, E.; Lee, C.; Prather, K. A.; Bertram, T. H. On the role of particle inorganic mixing state in the reactive uptake of N_2O_5 to ambient aerosol particles. *Environ. Sci. Technol.* **2014**, *48* (3), 1618−1627.
(46) Allen, H. C.; Laux, J. M.; Vogt, R.; FinlaysonPitts, B. J.; Hemminger, J. C. Water-induced reorganization of ultrathin nitrate films on NaCl: implications for the tropospheric chemistry of sea salt particles. *J. Phys. Chem.* **1996**, *100* (16), 6371−6375.
(47) Bertram, T. H.; Thornton, J. A. Toward a general parameterization of N_2O_5 reactivity on aqueous particles: the competing effects of particle liquid water, nitrate and chloride. *Atmos. Chem. Phys.* **2009**, *9* (21), 8351−8363.
(48) Bertram, T. H.; Thornton, J. A.; Riedel, T. P.; Middlebrook, A. M.; Bahreini, R.; Bates, T. S.; Quinn, P. K.; Coffman, D. J. Direct observations of N_2O_5 reactivity on ambient aerosol particles. *Geophys. Res. Lett.* **2009**, *36*, (19); DOI: 10.1029/2009GL040248.
(49) Matsumoto, K.; Minami, H.; Uyama, Y.; Uematsu, M. Size partitioning of particulate inorganic nitrogen species between the fine and coarse mode ranges and its implication to their deposition on the surface ocean. *Atmos. Environ.* **2009**, *43* (28), 4259−4265.
(50) Gantt, B.; Kelly, J. T.; Bash, J. O. Updating sea spray aerosol emissions in the Community Multiscale Air Quality (CMAQ) model version 5.0.2. *Geosci. Model Dev.* **2015**, *8* (11), 3733−3746.
(51) Foner, H. A.; Ganor, E. The chemical and mineralogical composition of some urban atmospheric aerosols in Israel. *Atmos. Environ., Part B* **1992**, *26* (1), 125−133.
(52) Dos Santos, M.; Dawidowski, L.; Smichowski, P.; Graciela Ulke, A.; Gomez, D. Factors controlling sea salt abundances in the urban atmosphere of a coastal South American megacity. *Atmos. Environ.* **2012**, *59*, 483−491.
(53) Makowski Giannoni, S.; Trachte, K.; Rollenbeck, R.; Lehnert, L.; Fuchs, J.; Bendix, J. Atmospheric salt deposition in a tropical mountain rainforest at the eastern Andean slopes of south Ecuador - Pacific or Atlantic origin? *Atmos. Chem. Phys.* **2016**, *16* (15), 10241−10261.
(54) Chalbot, M. C.; McElroy, B.; Kavouras, I. G. Sources, trends and regional impacts of fine particulate matter in southern Mississippi valley: significance of emissions from sources in the Gulf of Mexico coast. *Atmos. Chem. Phys.* **2013**, *13* (7), 3721−3732.
(55) O'Brien, R. E.; Wang, B.; Laskin, A.; Riemer, N.; West, M.; Zhang, Q.; Sun, Y.; Yu, X.-Y.; Alpert, P.; Knopf, D. A.; Gilles, M. K.; Moffet, R. C. Chemical imaging of ambient aerosol particles: observational constraints on mixing state parameterization. *J. Geophys. Res.: Atmos.* **2015**, *120* (18), 9591−9605.
(56) Moffet, R. C.; Roedel, T. C.; Kelly, S. T.; Yu, X. Y.; Carroll, G. T.; Fast, J.; Zaveri, R. A.; Laskin, A.; Gilles, M. K. Spectro-microscopic measurements of carbonaceous aerosol aging in central California. *Atmos. Chem. Phys.* **2013**, *13* (20), 10445−10459.
(57) Shaw, G. E. Aerosol chemical-components in Alaska air masses. 2. Sea salt and marine product. *J. Geophys. Res.* **1991**, *96* (D12), 22369−22372.
(58) Udisti, R.; Dayan, U.; Becagli, S.; Busetto, M.; Frosini, D.; Legrand, M.; Lucarelli, F.; Preunkert, S.; Severi, M.; Traversi, R.; Vitale, V. Sea spray aerosol in central Antarctica. Present atmospheric behaviour and implications for paleoclimatic reconstructions. *Atmos. Environ.* **2012**, *52*, 109−120.

DOI: 10.1021/acs.est.7b02085
Environ. Sci. Technol. 2017, 51, 9533−9542

(59) Hara, K.; Osada, K.; Kido, M.; Hayashi, M.; Matsunaga, K.; Iwasaka, Y.; Yamanouchi, T.; Hashida, G.; Fukatsu, T. Chemistry of sea-salt particles and inorganic halogen species in Antarctic regions: compositional differences between coastal and inland stations. *J. Geophys. Res.* **2004**, *109*, (D20); DOI: 10.1029/2004JD004713.
(60) Silva, B.; Rivas, T.; Garcia-Rodeja, E.; Prieto, B. Distribution of ions of marine origin in Galicia (NW Spain) as a function of distance from the sea. *Atmos. Environ.* **2007**, *41* (21), 4396−4407.
(61) Gustafsson, M. E. R.; Franzen, L. G. Inland transport of marine aerosols in southern Sweden. *Atmos. Environ.* **2000**, *34* (2), 313−325.
(62) Manders, A. M. M.; Schaap, M.; Querol, X.; Albert, M. F. M. A.; Vercauteren, J.; Kuhlbusch, T. A. J.; Hoogerbrugge, R. Sea salt concentrations across the European continent. *Atmos. Environ.* **2010**, *44* (20), 2434−2442.
(63) Ueda, S.; Hirose, Y.; Miura, K.; Okochi, H. Individual aerosol particles in and below clouds along a Mt. Fuji slope: modification of sea-salt-containing particles by in-cloud processing. *Atmos. Res.* **2014**, *137*, 216−227.
(64) Pilson, M. E. Q. *An Introduction to the Chemistry of the Sea*; Prentice Hall: 1998.
(65) Sullivan, R. C.; Guazzotti, S. A.; Sodeman, D. A.; Prather, K. A. Direct observations of the atmospheric processing of Asian mineral dust. *Atmos. Chem. Phys.* **2007**, *7*, 1213−1236.
(66) Moffet, R. C.; Desyaterik, Y.; Hopkins, R. J.; Tivanski, A. V.; Gilles, M. K.; Wang, Y.; Shutthanandan, V.; Molina, L. T.; Abraham, R. G.; Johnson, K. S.; Mugica, V.; Molina, M. J.; Laskin, A.; Prather, K. A. Characterization of aerosols containing Zn, Pb, and Cl from an industrial region of Mexico City. *Environ. Sci. Technol.* **2008**, *42* (19), 7091−7097.
(67) Ault, A. P.; Axson, J. L. Atmospheric aerosol chemistry: spectroscopic and microscopic advances. *Anal. Chem.* **2017**, *89* (1), 430−452.
(68) Noble, C. A.; Prather, K. A. Real-time single particle monitoring of a relative increase in marine aerosol concentration during winter rainstorms. *Geophys. Res. Lett.* **1997**, *24* (22), 2753−2756.
(69) Ault, A. P.; Zhao, D.; Ebben, C. J.; Tauber, M. J.; Geiger, F. M.; Prather, K. A.; Grassian, V. H. Raman microspectroscopy and vibrational sum frequency generation spectroscopy as probes of the bulk and surface compositions of size-resolved sea spray aerosol particles. *Phys. Chem. Chem. Phys.* **2013**, *15* (17), 6206−6214.
(70) Guasco, T. L.; Cuadra-Rodriguez, L. A.; Pedler, B. E.; Ault, A. P.; Collins, D. B.; Zhao, D.; Kim, M. J.; Ruppel, M. J.; Wilson, S. C.; Pomeroy, R. S.; Grassian, V. H.; Azam, F.; Bertram, T. H.; Prather, K. A. Transition metal associations with primary biological particles in sea spray aerosol generated in a wave channel. *Environ. Sci. Technol.* **2014**, *48* (2), 1324−1333.
(71) Prather, K. A.; Bertram, T. H.; Grassian, V. H.; Deane, G. B.; Stokes, M. D.; DeMott, P. J.; Aluwihare, L. I.; Palenik, B. P.; Azam, F.; Seinfeld, J. H.; Moffet, R. C.; Molina, M. J.; Cappa, C. D.; Geiger, F. M.; Roberts, G. C.; Russell, L. M.; Ault, A. P.; Baltrusaitis, J.; Collins, D. B.; Corrigan, C. E.; Cuadra-Rodriguez, L. A.; Ebben, C. J.; Forestieri, S. D.; Guasco, T. L.; Hersey, S. P.; Kim, M. J.; Lambert, W. F.; Modini, R. L.; Mui, W.; Pedler, B. E.; Ruppel, M. J.; Ryder, O. S.; Schoepp, N. G.; Sullivan, R. C.; Zhao, D. Bringing the ocean into the laboratory to probe the chemical complexity of sea spray aerosol. *Proc. Natl. Acad. Sci. U. S. A.* **2013**, *110* (19), 7550−7555.
(72) Laskin, A.; Iedema, M. J.; Cowin, J. P. Quantitative time-resolved monitoring of nitrate formation in sea salt particles using a CCSEM/EDX single particle analysis. *Environ. Sci. Technol.* **2002**, *36* (23), 4948−4955.
(73) Ault, A. P.; Moffet, R. C.; Baltrusaitis, J.; Collins, D. B.; Ruppel, M. J.; Cuadra-Rodriguez, L. A.; Zhao, D.; Guasco, T. L.; Ebben, C. J.; Geiger, F. M.; Bertram, T. H.; Prather, K. A.; Grassian, V. H. Size-dependent changes in sea spray aerosol composition and properties with different seawater conditions. *Environ. Sci. Technol.* **2013**, *47* (11), 5603−5612.
(74) Geng, H.; Hwang, H.; Liu, X.; Dong, S.; Ro, C. U. Investigation of aged aerosols in size-resolved Asian dust storm particles transported from Beijing, China, to Incheon, Korea, using low-Z particle EPMA. *Atmos. Chem. Phys.* **2014**, *14* (7), 3307−3323.
(75) Sobanska, S.; Coeur, C.; Maenhaut, W.; Adams, F. SEM-EDX characterisation of tropospheric aerosols in the Negev desert (Israel). *J. Atmos. Chem.* **2003**, *44* (3), 299−322.
(76) Ali, H. M.; Iedema, M.; Yu, X. Y.; Cowin, J. P. Ionic strength dependence of the oxidation of SO_2 by H_2O_2 in sodium chloride particles. *Atmos. Environ.* **2014**, *89*, 731−738.
(77) Laskin, A.; Wang, H.; Robertson, W. H.; Cowin, J. P.; Ezell, M. J.; Finlayson-Pitts, B. J. A new approach to determining gas-particle reaction probabilities and application to the heterogeneous reaction of deliquesced sodium chloride particles with gas-phase hydroxyl radicals. *J. Phys. Chem. A* **2006**, *110* (36), 10619−10627.
(78) Laskin, A.; Iedema, M. J.; Cowin, J. P. Time-resolved aerosol collector for CCSEM/EDX single-particle analysis. *Aerosol Sci. Technol.* **2003**, *37* (3), 246−260.
(79) Allen, H. M.; Draper, D. C.; Ayres, B. R.; Ault, A. P.; Bondy, A. L.; Takahama, S.; Modini, R. L.; Baumann, K.; Edgerton, E.; Knote, C.; Laskin, A.; Wang, B.; Fry, J. L. Influence of crustal dust and sea spray supermicron particle concentrations and acidity on inorganic NO_3^- aerosol during the 2013 Southern Oxidant and Aerosol Study. *Atmos. Chem. Phys.* **2015**, *15* (18), 10669−10685.
(80) Craig, R. L.; Bondy, A. L.; Ault, A. P. Computer-controlled Raman microspectroscopy (CC-Raman): a method for the rapid characterization of individual atmospheric aerosol particles. *Aerosol Sci. Technol.*, **2017**. DOI: 10.1080/02786826.2017.1337268
(81) Hidy, G. M.; Blanchard, C. L.; Baumann, K.; Edgerton, E.; Tanenbaum, S.; Shaw, S.; Knipping, E.; Tombach, I.; Jansen, J.; Walters, J. Chemical climatology of the southeastern United States, 1999−2013. *Atmos. Chem. Phys.* **2014**, *14* (21), 11893−11914.
(82) Marple, V. A.; Rubow, K. L.; Behm, S. M. A microorifice uniform deposit impactor (MOUDI)-description, calibration and use. *Aerosol Sci. Technol.* **1991**, *14* (4), 434−446.
(83) Budisulistiorini, S. H.; Li, X.; Bairai, S. T.; Renfro, J.; Liu, Y.; Liu, Y. J.; McKinney, K. A.; Martin, S. T.; McNeill, V. F.; Pye, H. O. T.; Nenes, A.; Neff, M. E.; Stone, E. A.; Mueller, S.; Knote, C.; Shaw, S. L.; Zhang, Z.; Gold, A.; Surratt, J. D. Examining the effects of anthropogenic emissions on isoprene-derived secondary organic aerosol formation during the 2013 Southern Oxidant and Aerosol Study (SOAS) at the Look Rock, Tennessee ground site. *Atmos. Chem. Phys.* **2015**, *15* (15), 8871−8888.
(84) Laskin, A.; Cowin, J. P.; Iedema, M. J. Analysis of individual environmental particles using modern methods of electron microscopy and X-ray microanalysis. *J. Electron Spectrosc. Relat. Phenom.* **2006**, *150* (2−3), 260−274.
(85) Ault, A. P.; Peters, T. M.; Sawvel, E. J.; Casuccio, G. S.; Willis, R. D.; Norris, G. A.; Grassian, V. H. Single-particle SEM-EDX analysis of iron-containing coarse particulate matter in an urban environment: sources and distribution of iron within Cleveland, Ohio. *Environ. Sci. Technol.* **2012**, *46* (8), 4331−4339.
(86) Shen, H. R.; Peters, T. M.; Casuccio, G. S.; Lersch, T. L.; West, R. R.; Kumar, A.; Kumar, N.; Ault, A. P. Elevated concentrations of lead in particulate matter on the neighborhood-scale in Delhi, India as determined by single particle analysis. *Environ. Sci. Technol.* **2016**, *50* (10), 4961−4970.
(87) Liu, D.-Y.; Rutherford, D.; Kinsey, M.; Prather, K. A. Real-time monitoring of pyrotechnically derived aerosol particles in the troposphere. *Anal. Chem.* **1997**, *69* (10), 1808−1814.
(88) Li, W. J.; Shi, Z. B.; Yan, C.; Yang, L. X.; Dong, C.; Wang, W. X. Individual metal-bearing particles in a regional haze caused by firecracker and firework emissions. *Sci. Total Environ.* **2013**, *443*, 464−469.
(89) Martin-Alberca, C.; Garcia-Ruiz, C. Analytical techniques for the analysis of consumer fireworks. *TrAC, Trends Anal. Chem.* **2014**, *56*, 27−36.
(90) Draxler, R. R.; Rolph, G. D. *HYSPLIT (HYbrid Single Particle Lagrangian Integrated Trajectory) v. 4.8 Model access via NOAA ARL READY Website*; NOAA Air Resources Laboratory, Silver Spring, MD, 2003.
(91) Wang, Y. Q.; Zhang, X. Y.; Draxler, R. R. TrajStat: GIS-based software that uses various trajectory statistical analysis methods to

identify potential sources from long-term air pollution measurement data. *Environ. Model. Softw.* **2009**, *24* (8), 938−939.
(92) DeMott, P. J.; Hill, T. C. J.; McCluskey, C. S.; Prather, K. A.; Collins, D. B.; Sullivan, R. C.; Ruppel, M. J.; Mason, R. H.; Irish, V. E.; Lee, T.; Hwang, C. Y.; Rhee, T. S.; Snider, J. R.; McMeeking, G. R.; Dhaniyala, S.; Lewis, E. R.; Wentzell, J. J. B.; Abbatt, J.; Lee, C.; Sultana, C. M.; Ault, A. P.; Axson, J. L.; Diaz Martinez, M.; Venero, I.; Santos-Figueroa, G.; Stokes, M. D.; Deane, G. B.; Mayol-Bracero, O. L.; Grassian, V. H.; Bertram, T. H.; Bertram, A. K.; Moffett, B. F.; Franc, G. D. Sea spray aerosol as a unique source of ice nucleating particles. *Proc. Natl. Acad. Sci. U. S. A.* **2016**, *113* (21), 5797−5803.
(93) Orellana, M. V.; Matrai, P. A.; Leck, C.; Rauschenberg, C. D.; Lee, A. M.; Coz, E. Marine microgels as a source of cloud condensation nuclei in the high Arctic. *Proc. Natl. Acad. Sci. U. S. A.* **2011**, *108* (33), 13612−13617.
(94) Newberg, J. T.; Matthew, B. M.; Anastasio, C. Chloride and bromide depletions in sea-salt particles over the northeastern Pacific Ocean. *J. Geophys. Res.: Atmos.* **2005**, *110* (D6), 13.
(95) Hoffman, R. C.; Laskin, A.; Finlayson-Pitts, B. J. Sodium nitrate particles: physical and chemical properties during hydration and dehydration, and implications for aged sea salt aerosols. *J. Aerosol Sci.* **2004**, *35* (7), 869−887.
(96) Ziemann, P. J.; McMurry, P. H. Spatial distribution of chemical components in aerosol particles as determined from secondary electron yield measurements: implications for mechanisms of multicomponent aerosol crystallization. *J. Colloid Interface Sci.* **1997**, *193* (2), 250−8.
(97) Guo, H.; Xu, L.; Bougiatioti, A.; Cerully, K. M.; Capps, S. L.; Hite, J. R., Jr.; Carlton, A. G.; Lee, S. H.; Bergin, M. H.; Ng, N. L.; Nenes, A.; Weber, R. J. Fine-particle water and pH in the southeastern United States. *Atmos. Chem. Phys.* **2015**, *15* (9), 5211−5228.
(98) Weber, R. J.; Guo, H. Y.; Russell, A. G.; Nenes, A. High aerosol acidity despite declining atmospheric sulfate concentrations over the past 15 years. *Nat. Geosci.* **2016**, *9* (4), 282−285.
(99) Rindelaub, J. D.; Craig, R. L.; Nandy, L.; Bondy, A. L.; Dutcher, C. S.; Shepson, P. B.; Ault, A. P. Direct measurement of pH in individual particles via raman microspectroscopy and variation in acidity with relative humidity. *J. Phys. Chem. A* **2016**, *120* (6), 911−917.
(100) Craig, R. L.; Nandy, L.; Axson, J. L.; Dutcher, C. S.; Ault, A. P. Spectroscopic determination of aerosol pH from acid-base equilibria in inorganic, organic, and mixed systems. *J. Phys. Chem. A* **2017**, DOI: 10.1021/acs.jpca.7b05261.
(101) Gurciullo, C.; Lerner, B.; Sievering, H.; Pandis, S. N. Heterogeneous sulfate production in the remote marine environment: cloud processing and sea-salt particle contributions. *J. Geophys. Res.: Atmos.* **1999**, *104* (D17), 21719−21731.
(102) Skinner, L. M.; Sambles, J. R. The Kelvin equation—a review. *J. Aerosol Sci.* **1972**, *3* (3), 199−210.
(103) McNeill, V. F.; Patterson, J.; Wolfe, G. M.; Thornton, J. A. The effect of varying levels of surfactant on the reactive uptake of N_2O_5 to aqueous aerosol. *Atmos. Chem. Phys.* **2006**, *6* (6), 1635−1644.
(104) Axson, J. L.; May, N. W.; Colon-Bernal, I. D.; Pratt, K. A.; Ault, A. P. Lake spray aerosol: a chemical signature from individual ambient particles. *Environ. Sci. Technol.* **2016**, *50* (18), 9835−9845.
(105) May, N. W.; Axson, J. L.; Watson, A.; Pratt, K. A.; Ault, A. P. Lake spray aerosol generation: a method for producing representative particles from freshwater wave breaking. *Atmos. Meas. Tech.* **2016**, *9* (9), 4311−4325.
(106) Nguyen, T. K. V.; Petters, M. D.; Suda, S. R.; Guo, H.; Weber, R. J.; Carlton, A. G. Trends in particle-phase liquid water during the Southern Oxidant and Aerosol Study. *Atmos. Chem. Phys.* **2014**, *14* (20), 10911−10930.
(107) Xiong, F.; McAvey, K. M.; Pratt, K. A.; Groff, C. J.; Hostetler, M. A.; Lipton, M. A.; Starn, T. K.; Seeley, J. V.; Bertman, S. B.; Teng, A. P.; Crounse, J. D.; Nguyen, T. B.; Wennberg, P. O.; Misztal, P. K.; Goldstein, A. H.; Guenther, A. B.; Koss, A. R.; Olson, K. F.; de Gouw, J. A.; Baumann, K.; Edgerton, E. S.; Feiner, P. A.; Zhang, L.; Miller, D. O.; Brune, W. H.; Shepson, P. B. Observation of isoprene hydroxynitrates in the southeastern United States and implications for the fate of NO_x. *Atmos. Chem. Phys.* **2015**, *15* (19), 11257−11272.
(108) Gantt, B.; Meskhidze, N. The physical and chemical characteristics of marine primary organic aerosol: a review. *Atmos. Chem. Phys.* **2013**, *13* (8), 3979−3996.

DOI: 10.1021/acs.est.7b02085
Environ. Sci. Technol. 2017, 51, 9533−9542